Nanotechnology **19** (2008) 395704 (7pp) doi:10.1088/0957-4484/19/39/395704

Conductivity of nanoporous InP membranes investigated using terahertz spectroscopy

S K E Merchant[1], J Lloyd-Hughes[1,3], L Sirbu[2], I M Tiginyanu[2], P Parkinson[1], L M Herz[1] and M B Johnston[1]

[1] Department of Physics, University of Oxford, Clarendon Laboratory, Parks Road, Oxford OX1 3PU, UK
[2] National Centre for Materials Study and Testing, Technical University of Moldova, and Institute of Applied Physics, Academy of Sciences of Moldova, Chisinau, MD-2004, Republic of Moldova

E-mail: s.merchant@physics.ox.ac.uk and m.johnston@physics.ox.ac.uk

Received 12 May 2008, in final form 7 July 2008
Published 11 August 2008
Online at stacks.iop.org/Nano/19/395704

Abstract
We have investigated the terahertz conductivity of extrinsic and photoexcited electrons in nanoporous indium phosphide (InP) at different pore densities and orientations. The form of electronic transport in the film was found to differ significantly from that for bulk InP. While photo-generated electrons showed Drude-like transport, the behaviour for extrinsic electrons deviated significantly from the Drude model. Time-resolved photoconductivity measurements found that carrier recombination was slow, with lifetimes exceeding 1 ns for all porosities and orientations. When considered together, these findings suggest that the surfaces created by the nanopores strongly alter the dynamics of both extrinsic and photoexcited electrons.

(Some figures in this article are in colour only in the electronic version)

1. Introduction

Since the discovery of the luminescent properties of electrochemically etched nanoporous silicon [1], porous semiconductors have become the focus of intense research [2–6]. This is due primarily to the significant differences between the properties of porous semiconductors and their bulk counterparts [7], and to the potential new applications that these properties afford. For example, recent studies have reported porosity-induced birefringence in GaP with potential applications in optoelectronics [8, 9], luminescence in porous III–V and II–VI semiconductors [10–12], the ability of porous III–Vs to support Fröhlich-type surface vibrations [13, 14], and a porosity-induced blueshift of photoluminescence in CdSe [15]. There have also been studies of terahertz emission from porous InP [16].

In order to exploit the potential of nanoporous materials it is important to develop an understanding of how nanoscale structure influences the dynamics of charge carriers. An ideal tool for accomplishing this is the technique of terahertz time-domain spectroscopy [17]. Terahertz pulses are well suited for the purpose of probing semiconductor carrier dynamics because their low energy is non-resonant with the bandgap, and carrier scattering rates and plasma frequencies typically fall in the terahertz range. An additional advantage of terahertz spectroscopy over electrical conductivity measurements is that it is not necessary to fabricate Ohmic contacts, which is particularly a problem for fragile porous membranes.

The frequency-dependent terahertz conductivity has been examined for a variety of bulk semiconductors [18] and nanostructures [19–21], and for some of these systems, the conductivity has also been measured as a function of time after the photoexcitation of carriers by a pulsed laser beam. The time-dependent conductivity yields insights into carrier recombination dynamics, where carrier lifetimes can be significantly shortened by the presence of surface defects [20, 22].

In this paper we report on the conductive response of carriers in porous InP films using terahertz time-domain

[3] Present address: ETH Zürich, Institute for Quantum Electronics, Wolfgang-Pauli-Strasse 16, 8093 Zürich, Switzerland.

spectroscopy. Initially, in section 2, we describe the fabrication and characterization of nanoporous InP films with different porosities and crystallographic orientations. We discuss our data analysis approach in section 3, before presenting the measured frequency-dependent dark conductivity and the time-resolved photoconductivity in section 4. The dark conductivity at terahertz frequencies does not correspond to the Drude model of free-carrier absorption, and is reduced significantly in comparison to that of bulk InP. In addition the measured electron recombination lifetime is longer than that of bulk InP, despite the large effective surface area created by the pores.

2. Experimental method

2.1. Sample fabrication and morphology

Crystalline (100)- and (111)-oriented substrates of S-doped n-InP with 500 μm thickness (prior to anodic etching) and free electron concentration of 1.3×10^{18} cm^{-3} were used. The anodization was carried out in an electrochemical double cell as described elsewhere [23]. A four-electrode configuration was used: a Pt reference electrode in the electrolyte, a Pt reference electrode on the sample, a Pt counter electrode, and a Pt working electrode. The temperature was kept constant with a thermostat. The electrolyte was pumped continuously through both parts of the double cell with the help of a peristaltic pump. All equipment involved in the experiments was computer-controlled. The area of the sample exposed to the electrolyte was 0.5 cm^2. The anodic etching was carried out in 5% HCl aqueous solution at room temperature in potentiostatic regime with the following values of the applied voltage: 3.0, 5.0 and 6.5 V, which resulted in low, medium and high degrees of porosity respectively. A TESCAN scanning electron microscope equipped with an Oxford Instruments INCA energy dispersive x-ray (EDX) system was used to analyse the morphology and chemical composition of the porous samples.

As shown earlier [2], two types of pores can be introduced in III–V semiconductor compounds: crystallographically-oriented or 'crysto' pores, and current-line-oriented or 'curro' pores. Crysto pores are usually generated at low anodization current densities or applied voltages, the mechanism of their formation being related to direct dissolution of the material. Curro pores are formed at relatively high anodic current densities or applied voltages, their growth being mediated by oxide formation and its dissolution at the pore tip [2].

Crysto pores grow along the $\langle 111 \rangle$ *B* directions of the zincblende structure [23]. The intersection of [111]- and $[1\bar{1}\bar{1}]$-oriented pores results in the formation of a 3D porous structure which can be easily evidenced under the applied voltage of 3 V. Increasing the applied voltage (and consequently the anodic current density) creates conditions for the formation of curro pores which are oriented along current lines and usually show circular shape, independent of the crystallographic orientation of the substrate. A fascinating property of the curro pores is their long range interaction in the process of formation, leading under certain conditions to self-arrangement of pores in a two-dimensional hexagonal close-packed lattice [24]. Several parameters such as the concentration and the temperature of the electrolyte as well as the applied voltage should be optimized to identify the conditions necessary for this self-arrangement.

2.2. Sample details

For this study, porous InP membranes were prepared in two sets. The first set, herein labelled set A, comprised three (100)-oriented samples of low, medium, and high porosities, with dimensional characteristics as summarized in figure 1. A scanning electron microscope image of a typical sample of each porosity is shown, and it can be seen from these images that it is not only the pore size and spacing that varies with applied voltage in the electrochemical cell, but also the variance of the pore size, and the order of the pore structure. Cross-sectional images of the samples showed that in the high and medium porosity samples, curro pores were grown, while in the low porosity sample, crysto pores were grown. The second set, herein labelled set B, comprised two samples of low porosity, one being (100)-oriented, and the other (111)-oriented. The porous membranes were 30 μm thick.

2.3. Experiment and system details

Each sample was mounted on a piece of aluminium with a hole of diameter 2.5 mm. The transmission of terahertz radiation through this hole was measured using a terahertz time-domain spectrometer similar to that described in [25]. A piece of aluminium with a 2.5 mm aperture was used in the place of the sample for the reference measurement. Time-domain data were recorded for each of the samples in both set A and set B over a time window of 60 ps. The use of optically thick emitter and detector materials ensured that no reflections internal to the spectrometer were present in this time range. From the time-domain data the frequency-dependent transmission was obtained by Fourier transform, with a spectral resolution of 17 GHz. Additionally, an optical-pump terahertz-probe spectrometer [20] was used to record the differential terahertz transmission through the samples under photoexcitation at 800 nm as a function of pump–probe delay time τ. Differential transmission data were recorded up to 1 ns after the photoexcitation of carriers for all samples in both sample sets. For all measurements, the terahertz electric field was linearly polarized, and the terahertz beam was normally incident on the sample surface. All measurements were performed at room temperature and with the terahertz path length under vacuum.

3. Data analysis

To calculate the complex conductivity of our samples from the measured terahertz time-domain data, we proceed as follows: the transmitted terahertz electric fields for the sample, $E_s(t)$, and for the reference, $E_r(t)$, are Fourier transformed to obtain the corresponding frequency-dependent electric fields $\tilde{E}_s(\omega)$ and $\tilde{E}_r(\omega)$. The transmission T_m is defined as

$$T_m(\omega) = \frac{\tilde{E}_s(\omega)}{\tilde{E}_r(\omega)}. \quad (1)$$

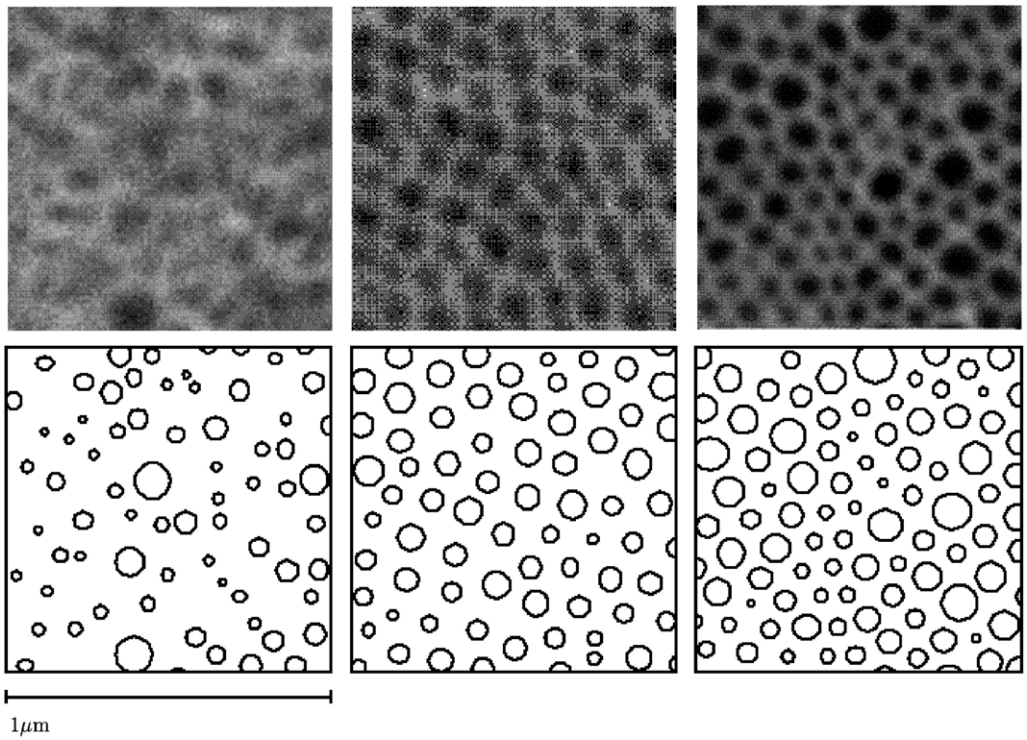

Figure 1. Scanning electron microscope images of typical porous InP membranes of low, medium and high porosities.

Table 1. The dimensional properties of typical porous InP membranes of low, medium and high porosities.

	Porosity		
	Low	Medium	High
Pore type	Crysto	Curro	Curro
Diameter (mean (nm)/variance (nm^2))	42/51	64/37	60/82
Inter-pore spacing (mean (nm)/variance (nm^2))	131/217	130/58	113/53
Pore density (μm^{-2})	68	68	86
Fill factor	0.90	0.80	0.76
Effective surface area factor	242	357	423

Then the complex refractive index is obtained through the numerical solution of

$$T_{\mathrm{m}}(\omega) = \frac{2\tilde{n}_2(\tilde{n}_1+\tilde{n}_3)}{(\tilde{n}_2+\tilde{n}_1)(\tilde{n}_2+\tilde{n}_3)} \exp\left[-\mathrm{i}(\tilde{n}_2-\tilde{n}_{\mathrm{v}})\frac{\omega L}{c}\right] \mathrm{FP}(\omega), \tag{2}$$

where the Fabry–Perot term is

$$\mathrm{FP}(\omega) = \left[1-\left(\frac{\tilde{n}_2-\tilde{n}_1}{\tilde{n}_2+\tilde{n}_1}\right)\left(\frac{\tilde{n}_2-\tilde{n}_3}{\tilde{n}_2+\tilde{n}_3}\right)\exp\left(-2\mathrm{i}\tilde{n}_2\frac{\omega L}{c}\right)\right]^{-1}. \tag{3}$$

In the above, $\tilde{n}_2$ is the complex refractive index of the sample, which is to be determined, $\tilde{n}_{1,3} = \tilde{n}_{\mathrm{v}} = 1$ are the complex refractive indices of the surrounding media (vacuum), L is the sample thickness and c is the speed of light.

There exists a simpler method that is commonly used to extract the complex refractive index of thin films from terahertz time-domain spectroscopy data, but this method is only valid in the thin film limit, that is, when

$$n_2 L\omega/c \ll 1. \tag{4}$$

For our samples $n_2 L\omega/c \simeq 2.2$, and so it is necessary to adopt a method that does not require this simplifying assumption. The numerical extraction method we adopted is based on that used by Duvillaret *et al* [26]. Alterations and extensions to this method were generally of a computational nature, but also included a change to the way the initial estimates of $\tilde{n}_2$ are used, to enable the program, in certain cases, to extract $\tilde{n}_2$ successfully when FP(ω) deviates substantially from 1.

The complex dielectric function may be obtained directly from the complex refractive index, and then used to find the complex conductivity, using

$$\epsilon = \epsilon_\infty + \mathrm{i}\frac{\sigma}{\epsilon_0\omega}. \tag{5}$$

The time-resolved photoconductivity $|\Delta\sigma(\tau)|$ is obtained from the differential terahertz transmission $\Delta T/T$ using

$$|\Delta\sigma(\tau)| = \frac{1+n_{\mathrm{s}}}{\delta Z_0}\frac{\Delta T}{T}, \tag{6}$$

where $\delta = 0.8$ μm is the thin film thickness, i.e. the thickness of the region containing photoexcited carriers, n_{s} is

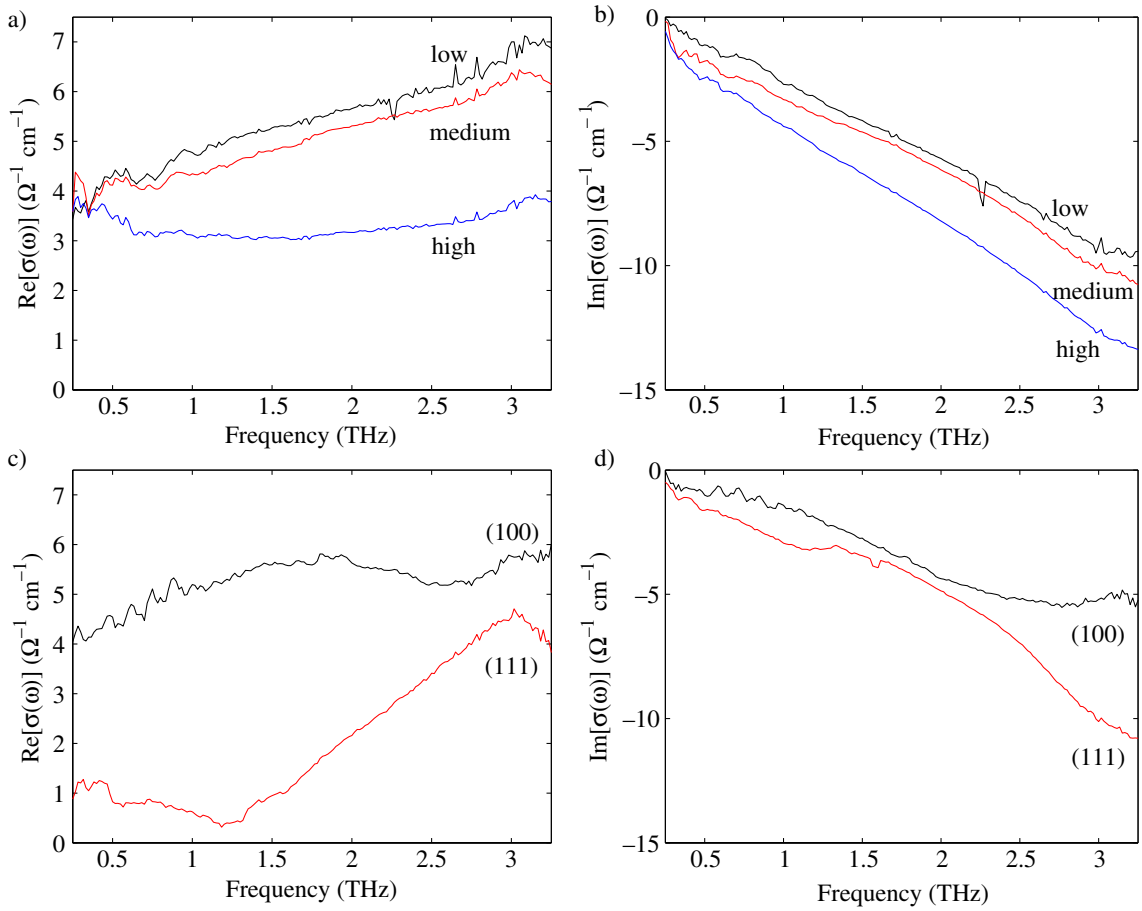

Figure 2. (a) Real and (b) imaginary components of the complex conductivity $\sigma(\omega)$ for (100)-oriented samples of high, medium and low porosity, and (c) Re$[\sigma(\omega)]$ and (d) Im$[\sigma(\omega)]$ for (100)- and (111)-oriented samples of low porosity, extracted numerically from terahertz time-domain spectroscopy data. A clear trend of decreasing Re$[\sigma(\omega)]$ with increasing porosity can be seen in (a). It can be seen from (c) that the (111)-oriented sample shows a strong suppression of Re$[\sigma(\omega)]$ below 3 THz.

the average refractive index of the nanoporous InP away from the photoexcited region, and Z_0 is the impedance of free space. The thin film limit (4) is applicable in this case—the thickness δ of the photoexcited region is much smaller than the sample thickness L.

4. Results

4.1. Dark conductivity

Figures 2(a) and (b) show the frequency-dependent conductivities extracted from the terahertz time-domain spectroscopy data for (100) nanoporous InP with different porosities (sample set A). Considering first the low porosity sample, the real part of the conductivity increases monotonically with frequency, and the imaginary component of the conductivity is negative and also increases in magnitude with frequency. This behaviour is very different from the conductivity predicted by the Drude model, which for a non-interacting electron gas predicts a peak in the real conductivity at zero frequency, and a positive imaginary component. Previous studies have shown that the conductivity of doped bulk semiconductors shows good agreement with the Drude model [18, 27]. For bulk InP with the same carrier density as these samples, $N = 1.3 \times 10^{18}$ cm^{-3}, the Drude model predicts a dc conductivity of the order $\sigma_0 \sim 10^3$ Ω^{-1} cm^{-1}, three orders of magnitude larger than the low-frequency conductivity seen here.

The real part of the conductivity is further suppressed at higher porosity, while the imaginary conductivity becomes increasingly negative (figures 2(a) and (b)). These trends in the conductivity correlate with the pore density, suggesting that the effective carrier density is being altered by the presence of surface-bound electronic states. Surface states pin the Fermi level at the surface, which in the case of n-InP bends the electronic bands upwards [28]. This band-bending results in an electron depletion layer close to the surface of the pores, which accounts for the low conductivity in our nanoporous samples. The volume of InP depleted of electrons increases with increasing porosity (owing to the increased surface area), which is consistent with the observed trend of increasing conductivity with decreasing porosity.

The influence of crystallographic orientation on the terahertz conductivity is shown in figures 2(c) and (d) for sample set B. For the (111)-oriented sample, the real component of the conductivity is suppressed over the whole frequency range in comparison to the (100)-oriented sample.

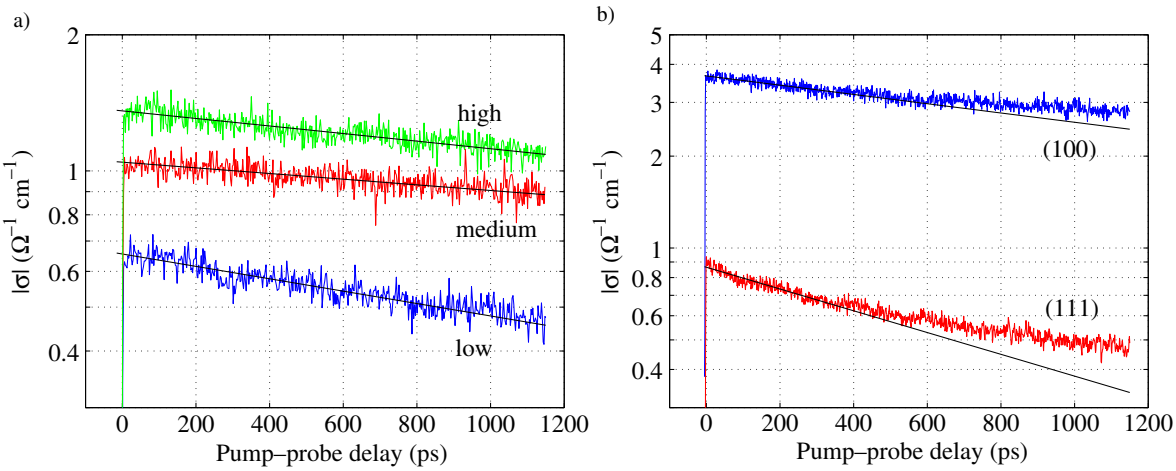

Figure 3. (a) Time-resolved photoconductivity, calculated from differential terahertz transmission data, for (100)-oriented samples of high, medium and low porosities. The photoconductivity increases with increasing porosity, and decays with lifetimes 3.2 ns, 6.9 ns and 5.2 ns for low, medium and high porosities respectively. (b) Photoconductivity for (100)- and (111)-oriented samples of low porosity. The photoconductivity decays with lifetimes 2.9 ns and 1.2 ns for (100)- and (111)-oriented respectively.

The suppression of the conductivity in sample set A and B is linked to the pore orientation: the reduction is strongest in the (111)-oriented sample, and in the high porosity (100)-oriented sample (which has curro pores). In these samples, the pore orientation is normal to the surface. The conductivity observed here is qualitatively consistent with observations of plasmonic behaviour in nanoscale semiconductors [20, 29], and this is discussed further in section 5.

4.2. Photoconductivity

The differential transmission was measured as described in section 2.3, then the photoconductivity $|\Delta\sigma(\tau)|$ was calculated from the differential transmission as described in section 3. The frequency-dependence of the ac conductivity (not shown) revealed a classical Drude-type transport behaviour [30]. The (frequency-averaged) photoconductivity of the samples in set A is shown in figure 3(a). The response of the photoexcited carriers is dominated by the electrons, because of the holes' low mobility. Unexpectedly, the photoconductivity increases with sample porosity. This is the opposite trend from that seen in the dark-conductivity experiments. It is tempting to attribute the enhanced conductivity to an increased mobility of photo-generated electrons alone. However it is important to note that the photoconductivity measured in our experiments is the *change* in conductivity induced by excitation with above bandgap photons. Since photoexcitation will significantly reduce the width of the surface depletion region (via screening), the conductivity of the extrinsic carriers will also be altered by the process of photoexcitation. Therefore, rather than the mobility of photo-generated electrons increasing with porosity, it is likely that the photo-induced reduction in the width of the surface depletion layer leads to an increase in the conductivity of extrinsic electrons. This explanation is consistent with the observed increase in photoconductivity with increasing porosity, since the effect of the depletion region on degrading the conductivity is most significant for the most porous samples. Thus any photo-induced reduction in the depletion width for these samples would cause the greatest increase in conductivity.

The observed carrier lifetimes are long: 3.17 ± 0.09 ns, 6.94 ± 0.43 ns and 5.20 ± 0.24 ns for low, medium and high porosities respectively. In comparison, a measurement of the carrier lifetime of photoexcited electrons in bulk InP gave a value of 330 ps. Surface traps provide recombination sites that strongly reduce the lifetime of electrons in bulk [22] and nanoscale [20] III–V semiconductors. It might therefore be expected that the larger surface area would result in an increased rate of carrier trapping, and a corresponding decrease in the lifetime, but this is not observed. The lifetime does not appear to be correlated with the effective surface area of the samples (figure 1), however there is a possible correlation with the pore diameter.

Similarly, the photoconductivities of the samples in set A, shown in figure 3(b), have long lifetimes: 6 ± 0.12 ns and 1.22 ± 0.02 ns for (100)- and (111)-oriented samples respectively. In the case of sample set B, the magnitude of the photoconductivity varies with orientation in the same way as the extrinsic carrier conductivity, i.e. in both cases, the conductivity of the (100)-oriented sample is greater.

5. Discussion

The previous sections described experiments that demonstrated that the conductivities of extrinsic and photoexcited electrons in nanoporous InP differ from those in bulk InP. In this section we discuss the possible origins of the observed conductive response. The shape of the extrinsic ac conductivity (figure 2) can be qualitatively accounted for by a surface plasmon model (see for example [20]) with a plasma frequency higher than the terahertz bandwidth of our system (as might be expected based on the plasma frequency in InP doped at 10^{18} cm^{-3}, which is roughly 10 THz). However, the observed ac conductivity of photoexcited carriers follows the Drude model [30], with

a carrier recombination lifetime longer than that of bulk InP (figure 3). This difference can be reconciled by the following consideration. Without photoexcitation, surface states create a depletion region close to the pores. Under a terahertz electric field extrinsic electrons are driven into the depletion region, thereby initiating surface plasmon oscillations. For the photoexcited case, with a sufficiently high carrier density the band is flattened at the surface [30], and the depletion region is removed. The ac conductivity then follows the Drude model, as the material is more similar to a bulk semiconductor.

6. Conclusions

We have measured the frequency-dependent extrinsic carrier conductivity and time-resolved photoconductivity of InP membranes of various degrees of porosity, and in two orientations. A non-Drude response was observed in the extrinsic carrier conductivity, while the photoconductivity exhibited Drude behaviour. This result is attributed to a depletion region close to the pore surface, which exists in the absence of photoexcitation, giving rise to surface plasmon oscillations, but which does not exist in the presence of a sufficiently high density of photocarriers, due to band-flattening. Measurements of the time-resolved frequency-averaged photoconductivity revealed that the carrier lifetime is substantially longer than that of bulk InP, which is inconsistent with the expectation that an increased surface area would result in the shortening of the carrier lifetime due to an increased number of surface traps.

Acknowledgments

This work was supported by INTAS under Grant No.05-104-7567. The authors from Oxford would also like to acknowledge financial support from the EPSRC.

References

[1] Canham L T 1990 Silicon quantum wire array fabrication by electrochemical and chemical dissolution of wafers *Appl. Phys. Lett.* **57** 1046–8
[2] Föll H, Langa S, Carstensen J, Christophersen M and Tiginyanu I M 2003 Pores in III–V semiconductors *Adv. Mater.* **15** 183–98
[3] Föll H, Christophersen M, Carstensen J and Hasse G 2002 Formation and application of porous silicon *Mater. Sci. Eng.* **39** 93–141
[4] Tiginyanu I M, Kravetsky I V, Monecke J, Cordts W, Marowsky G and Hartnagel H L 2000 Semiconductor sieves as nonlinear optical materials *Appl. Phys. Lett.* **77** 2415–7
[5] Christophersen M, Langa S, Carstensen J, Tiginyanu I M and Föll H 2003 A comparison of pores in silicon and pores in III–V compound materials *Phys. Status Solidi* a **197** 197–203
[6] Föll H, Carstensen J, Langa S, Christophersen M and Tiginyanu I M 2003 Porous III–V compound semiconductors: formation, properties, and comparison to silicon *Phys. Status Solidi* a **197** 61–70
[7] Föll H, Langa S, Carstensen J, Christophersen M, Lölkes S and Tiginyanu I M 2003 Engineering porous III–Vs *III–Vs Review* vol 16 pp 42–3
[8] Ursaki V V, Syrbu N N, Albu S, Zalamai V V, Tiginyanu I M and Boyd R W 2005 Artificial birefringence introduced by porosity in GaP *Semicond. Sci. Technol.* **20** 745–8
[9] Tiginyanu I M, Kravetsky I V, Langa S, Marowsky G, Monecke J and Föll H 2003 Porous III–V compounds as nonlinear optical materials *Phys. Status Solidi* a **197** 549–55
[10] Stevens-Kalceff M A, Tiginyanu I M, Langa S, Föll H and Hartnagel H L 2001 Correlation between morphology and cathodoluminescence in porous GaP *J. Appl. Phys.* **89** 2560–5
[11] Schmuki P, Lockwood D J, Labbe H J and Fraser J W 1996 Visible photoluminescence from porous GaAs *Appl. Phys. Lett.* **69** 1620–2
[12] Monaico E, Ursaki V V, Urbieta A, Fernandez P, Piqueras J, Boyd R W and Tiginyanu I M 2004 Porosity-induced gain of luminescence in CdSe *Semicond. Sci. Technol.* **19** L121–3
[13] Ursaki V V, Tiginyanu I M, Ricci P C, Anedda A, Foca E V and Syrbu N N 2001 Temperature dependence of raman scattering in porous gallium phosphide *J. Phys.: Condens. Matter* **13** 4579–89
[14] Sarua A, Monecke J, Irmer G, Tiginyanu I M, Gartner G and Hartnagel H L 2001 Fröhlich modes in porous III–V semiconductors *J. Phys.: Condens. Matter* **13** 6687–706
[15] Monaico E, Ursaki V V, Tiginyanu I M, Dashevsky Z, Kasiyan V and Boyd R W 2006 Porosity-induced blueshift of photoluminescence in CdSe *J. Appl. Phys.* **100** 053517
[16] Reid M, Cravetchi I V, Fedosejevs R, Tiginyanu I M and Sirbu L 2005 Enhanced terahertz emission from porous InP(111) membranes *Appl. Phys. Lett.* **86** 021904
[17] Schmuttenmaer C A 2004 Exploring dynamics in the far-infrared with terahertz spectroscopy *Chem. Rev.* **104** 1759–79
[18] Grischkowsky D, Keiding S, van Exter M and Fattinger C 1990 Far-infrared time-domain spectroscopy with terahertz beams of dielectrics and semiconductors *J. Opt. Soc. Am.* B **7** 2006–15
[19] Kaindl R A, Carnahan M A, Hagele D, Lovenich R and Chemla D S 2003 Ultrafast terahertz probes of transient conducting and insulating phases in an electron–hole gas *Nature* **423** 734–8
[20] Parkinson P, Lloyd-Hughes J, Gao Q, Tan H H, Jagadish C, Johnston M B and Herz L M 2007 Transient terahertz conductivity of GaAs nanowires *Nano Lett.* **7** 2162–5
[21] Beard M C, Turner G M and Schmuttenmaer C A 2002 Size-dependent photoconductivity in CdSe nanoparticles as measured by time-resolved terahertz spectroscopy *Nano Lett.* **2** 983–7
[22] Lloyd-Hughes J, Merchant S K E, Fu L, Tan H H, Jagadish C, Castro-Camus E and Johnston M B 2006 Influence of surface passivation on ultrafast carrier dynamics and terahertz radiation generation in GaAs *Appl. Phys. Lett.* **89** 232102
[23] Langa S, Carstensen J, Christophersen M, Föll H and Tiginyanu I M 2001 Observation of crossing pores in anodically etched n-GaAs *Appl. Phys. Lett.* **78** 1074–6
[24] Langa S, Tiginyanu I M, Carstensen J, Christophersen M and Föll H 2003 Self-organized growth of single crystals of nanopores *Appl. Phys. Lett.* **82** 278–80
[25] Johnston M B, Herz L M, Khan A L T, Kohler A, Davies A G and Linfield E H 2003 Low-energy vibrational modes in phenylene oligomers studied by THz time-domain spectroscopy *Chem. Phys. Lett.* **377** 256–62

[26] Duvillaret L, Garet F and Coutaz J-L 1996 A reliable method for extraction of material parameters in terahertz time-domain spectroscopy *IEEE J. Sel. Top. Quantum Electron.* **2** 739–46

[27] Nashima S, Morikawa S, Takata K and Hangyo M 2001 Measurement of optical properties of highly doped silicon by terahertz time domain reflection spectroscopy *Appl. Phys. Lett.* **79** 3923–5

[28] Hwang J S, Chou W Y, Hung M C, Wang J S and Lin H H 1997 Built-in electric field and surface Fermi level in InP surface-intrinsic n^+ structures by modulation spectroscopy *J. Appl. Phys.* **82** 3888–90

[29] Nienhuys H-K and Sundstrom V 2005 Influence of plasmons on terahertz conductivity measurements *Appl. Phys. Lett.* **87** 012101

[30] Lloyd-Hughes J, Merchant S K E, Sirbu L, Tiginyanu I M and Johnston M B 2008 unpublished